

A Phoswich Detector with Compton Suppression Capability for Radioxenon Measurements

A.T. Farsoni, Member IEEE, B. Alemayehu, A. Alhawsawi, E.M. Becker

Abstract– A phoswich detector with Compton suppression capability has been developed and tested for measuring xenon radioisotopes via a beta-gamma coincidence measurement technique. The phoswich detector has been designed with three scintillation layers. Beta-gamma coincidence events from radioxenon isotopes are identified when a coincidence energy absorption is detected in the first (BC-400) and second (CsI(Tl) crystal) scintillation layers. To identify and reject scattered photons from the CsI(Tl) crystal, the crystal is surrounded by a BGO scintillation layer. Our measurements show that the Compton suppression mechanism reduces the Compton continuum from 662 keV photons by 20%-50% in the low-energy region of spectrum. Our beta-gamma coincidence measurements with ^{135}Xe and ^{133}Xe radioisotopes show energy resolutions (FWHM) of 13%, 46% and 24% for 250 keV, 30keV and 80 keV gamma-ray peaks, respectively. In this paper, the detector design, assembly steps, digital pulse shape discrimination technique, and our recent measurements with radioactive lab sources and xenon radioisotopes are discussed.

Index Terms– Pulse Shape Discrimination, Compton Suppression, Phoswich Detector, Radioxenon Measurement.

I. INTRODUCTION

The International Monitoring System (IMS) has been established to install and employ radioxenon detectors in various locations to measure atmospheric concentration of xenon radioisotopes for any signs of nuclear weapon tests. Table 1 lists characteristic energies for the decay of $^{131\text{m}}\text{Xe}$, $^{133\text{m}}\text{Xe}$, ^{133}Xe , and ^{135}Xe [1]. Several radioxenon detectors have been designed and tested during the last two decades. The Swedish Automatic Unit for Noble gas Acquisition (SAUNA) [2], the SPLAX unit [3] and Automated Radioxenon Sampler and Analyzer (ARSA) [4-5] are among these detection systems. Except the SPLAX unit which uses a high-purity germanium detector to detect only X-rays and gamma-rays, the SAUNA and ARSA systems are designed based on a beta/gamma coincidence measurement technique. In this technique, beta particles (or conversion electrons) and gamma-rays (or X-rays) emitted from the source must be detected and measured simultaneously.

In a beta/gamma coincidence detection system, a beta/gamma coincidence spectrum is constructed to locate three regions of interest in which the four xenon radioisotopes can be detected and measured [4]. These regions are located at three x-ray/gamma-ray energy regions: 30, 81 and 250 keV.

One important parameter in evaluating the sensitivity of these systems for radioxenon measurement is the Minimum Detectable Concentration (MDC) for each radioxenon isotope in the atmosphere. The design criterion for all of these radioxenon detectors is that the MDC of ^{133}Xe should be 1mBq m^{-3} or less for a 24-hour sampling period [6]. The system's MDC for a particular xenon radioisotope can be improved by reducing the gamma-ray background in the regions of interest. It has been shown that using beta-gamma coincidence counting provides a 10^3 - to 10^4 -fold background reduction over standard gamma-ray spectroscopy [5].

Although employing a beta/gamma coincidence counting effectively rejects most of the single-event external gamma background, there is still some probability for high-energy gamma-rays from the source (emitted in coincidence with beta-particles or conversion electrons) to be Compton scattered in the gamma detector. These events produce an unwanted Compton background for the lower energy region of the gamma/beta coincidence spectra and can degrade the system's MDC [7].

TABLE 1
HALF-LIVES AND CHARACTERISTIC ENERGIES FOR THE DECAY OF $^{131\text{m}}\text{Xe}$, $^{133\text{m}}\text{Xe}$, ^{133}Xe , AND ^{135}Xe [1]

Nuclide	$^{131\text{m}}\text{Xe}$	$^{133\text{m}}\text{Xe}$	^{133}Xe	^{135}Xe
Half-life	11.93 d	2.19 d	5.25 d	9.14 h
Gamma-rays (keV)	163.9	233.2	81.0	250.0
Gamma-ray abundance (%)	1.96	10.3	37.0	90.0
X-ray, K-shell (keV)	30.	30.	31.	31.
X-ray abundance (%)	54.1	56.3	48.9	5.2
Beta, Max. Energy (keV)	-	-	346.	905.
Beta abundance (%)	-	-	99.	97.
CE, K-shell (keV)	129.	199.	45.	214.
CE abundance (%)	60.7	63.1	54.1	5.7

Manuscript received XXX, 2011. This work was supported by the U.S. Department of Energy, National Nuclear Security Administration under Contract No. DE-AC52-09NA29324.

The authors are with the Department of Nuclear Engineering and Radiation Health Physics, Oregon State University, Corvallis, OR 97331, USA. (telephone: 541-737-9645, email: abi.farsoni@oregonstate.edu)

In this work, a phoswich detector with three scintillating layers has been designed and evaluated for measuring xenon radioisotopes via a beta/gamma coincidence technique. One important feature of this detector in enhancing radioxenon detection is its capability to identify and reject Compton

scattering events in its gamma detection layer. The Compton suppression mechanism is integrated into the phoswich design and does not require a secondary detector.

In this paper, the detector design, assembly steps, digital pulse shape discrimination technique, and our recent measurements with radioactive lab sources and xenon radioisotopes produced in the TRIGA reactor at Oregon State University will be discussed. Accurate calculation of the MDC for the xenon radioisotopes requires knowledge of the various background components in a given spectrum and employing a xenon collection and purification system with the detector [7]. Thus, lacking the xenon collection and purification system, MDC calculations were not performed in this work and will instead be addressed in future research.

II. BACKGROUND

The combination of two or three dissimilar scintillators optically coupled to a photon detector such as a Photomultiplier Tube (PMT) is commonly called a “phoswich” (phosphor sandwich) detector. The scintillators are chosen to have different decay times so that the shape of the output pulse from the photomultiplier tube is dependent on the relative contribution of scintillation light from each scintillator. Two common applications of phoswich detectors are simultaneous detection of different radiation types and minimizing the background radiation in a radiation field of interest [8-12]. In both applications, scintillation layers are chosen because of their relative sensitivity to a particular radiation type. Then, independent measurements of the energy deposited in each scintillator can be obtained without the need for a second photomultiplier tube.

With phoswich detectors, pulse-shape discrimination (PSD) identifies the signals from each scintillator, thus identifying in which scintillator the energy deposition event occurred. Rise-time measurement is one of the most popular techniques to discriminate pulses from a phoswich detector [8, 9]. This technique is based upon integration of the anode pulse, followed by the determination of the time at which this integral reaches a certain fraction of its maximum (e.g. 10% to 90% of the maximum). An analog pulse-shape analyzer is used to measure this time interval, which is proportional to the decay time of the scintillator. This method, however, is useful only when the anode pulse decays with a single timing component. In coincidence measurements, where the incident radiations (e.g. beta particle and gamma ray) simultaneously interact with more than one scintillator, the resulting signal pulse will have more than one light-decay component, and therefore this technique cannot be applied for pulse shape discrimination.

The majority of PSD systems operate on analog signal pulses. However, more sophisticated analyses are possible with the use of digital signal processing. With the development of very fast ADCs, digital signal processing

methods have gained popularity for analyzing signals from radiation detectors [13-16].

Phoswich detectors have recently been considered as an alternative to simplify radioxenon detection [17-18]. Employing a phoswich detector and digital pulse-shape analysis, coincidence beta-gamma events from xenon radioisotopes can be measured with MDCs comparable to those of standard detection systems [18].

III. PHOSWICH DESIGN AND ASSEMBLY

A phoswich detector has been designed (Fig. 1) with three scintillation layers: a thin plastic scintillator (BC-400) to detect beta and conversion electrons, a CsI(Tl) crystal for measuring X-rays and gamma-rays and a BGO crystal, which surrounds the CsI(Tl) layer, to identify scattered photons and ultimately to reduce the Compton continuum in the gamma energy spectrum.

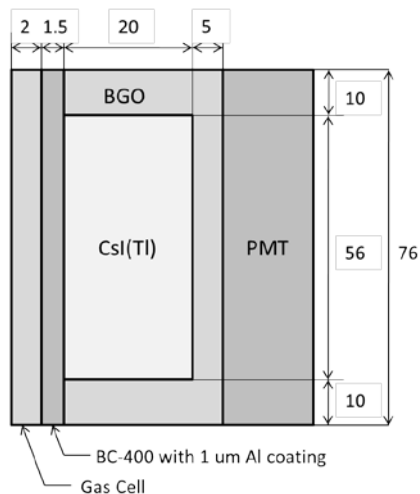


Fig. 1. Schematic diagram of the phoswich detector. All dimensions are in mm.

Our MCNP modeling with the design shown in Fig. 1 shows that the interaction probability of photons emitted from xenon radioisotopes (30, 81, and 250 keV) in the BC400 is less than 1.8%. Because of its low atomic numbers, Compton scattering is the dominant interaction in the BC400. This probability is above 87% in the CsI(Tl) crystal. Physical properties of the scintillators used in the phoswich detector are summarized in Table 2.

TABLE 2
PHYSICAL PROPERTIES OF SCINTILLATORS USED IN THE
PHOSWICH DETECTOR [18]

Scintillator	BC400	CsI(Tl)	BGO
Decay Time (ns)	2.4	~1000	300
Light Output (photon/MeV)	13,000	65,000	8,200
Peak Emission (nm)	423	540	480
Refractive Index	1.58	1.8	2.15
Density (g/cm ³)	1.032	4.51	7.13

The BGO crystal is a high-density (7.13 g/cm^3), high-efficiency scintillator and is commonly used in Compton suppression systems [19]. This scintillator is integrated into the phoswich detector to identify and reject unwanted Compton events in the CsI(Tl) crystal from internal and external gamma-ray sources. The decay time of BGO (300 ns) is different enough from the other two scintillators (2.4 ns of BC-400 and $\sim 1,000 \text{ ns}$ of CsI(Tl)) to enable our digital pulse-shape analysis algorithm to determine the origin of radiation interactions.

Previous tests on the Automated Radioxenon Sampler and Analyzer (ARSA) [20] have shown that latent radioxenon remains in the gas cells even after evacuation of the gases, leading to a memory effect which increases the background level for subsequent measurements. Therefore, to minimize this effect [21], a very thin layer of aluminum ($1 \mu\text{m}$) was deposited on the surface of the plastic scintillator. The aluminum coating was applied using a vacuum coating process at Oregon State University.



Fig. 2. The phoswich assembly wrapped with Teflon tape.

To have flexibility in customizing the phoswich detector, it was assembled in our lab by first smearing a layer of silicone grease (BC 630, Saint Gobain Crystals) inside the BGO crystal. The CsI(Tl) was then placed inside the BGO's hole and rotated in order to remove any remaining air bubbles and uniformly distribute the silicone grease between the crystals, thus forming a good optical coupling. The gaps between the BC-400 and BGO-CsI(Tl) layers and between the BGO and the PMT (R1307-07, Hamamatsu) glass window were also filled with a thin layer of silicone grease. The PMT and scintillators were wrapped with 5 layers of Teflon as shown in Fig. 2. The PMT and scintillators were then wrapped with plastic wrap to maintain the integrity of the assembly. Then, the whole scintillation assembly was fastened inside a custom aluminum housing.

IV. COMPTON SUPPRESSION MECHANISM

Major gamma interaction scenarios in the phoswich detector from internal and external gamma-ray sources are illustrated in Fig. 3. Photons emitted from the sample source in scenarios "a", "b" and "c" are assumed to be in coincidence with a beta absorption in the BC-400 layer. In scenario "a", a gamma-ray from the sample source undergoes a photoelectric interaction

and is fully absorbed in the CsI(Tl) crystal. If the resulting slow pulse ($\sim 1000 \text{ ns}$ decay time) is accompanied by a fast component from the BC-400 layer, the pulse will be identified as a valid beta/gamma coincidence event and the corresponding energy bin will be recorded in the two-dimensional energy spectrum. A single gamma-ray may also generate such a coincidence pulse when it is fully absorbed in the CsI(Tl) after a scatter in the BC-400 layer. Since the plastic has a low Z and is very thin, the probability of this event is low [22]. In scenarios "b" and "c", a gamma-ray from the source is scattered in the CsI(Tl) crystal and will be either absorbed or scattered, respectively, in the BGO crystal. When accompanied with a coincident beta absorption in the BC-400 layer, interaction scenarios "b" and "c" generate coincident pulses which are most likely responsible for Compton background in the two-dimensional beta/gamma coincidence spectrum. These events can be identified and rejected (suppressed) by our digital pulse shape discrimination analysis.

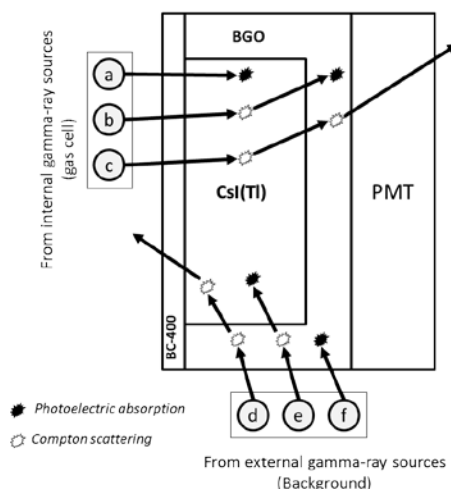


Fig. 3. Major interaction scenarios from internal and external gamma-ray sources in the phoswich detector. When accompanied with a coincident beta absorption in plastic scintillator, interaction scenarios "b" and "c" generate coincident pulses which are most likely responsible for Compton background in the two-dimensional beta/gamma coincidence spectrum. Corresponding pulses will be identified and rejected in our digital pulse shape discrimination analysis.

One other advantage of using a BGO crystal in this phoswich detector is to shield the CsI(Tl) crystal against background sources. Scenarios "d", "e" and "f" in Fig. 3 show some events in which external gamma-rays from background radiation interact with the phoswich detector. In scenarios "d" and "e", a gamma-ray from the external source is scattered in the BGO crystal and will be either absorbed or scattered in the CsI(Tl) crystal. In scenario "f", with no scattering, the external gamma-ray is fully absorbed in the BGO crystal. By identifying the BGO's timing component, pulses resulting from these scenarios are also rejected and will not contribute to the beta-gamma coincidence energy spectra.

V. DIGITAL PULSE PROCESSING

Fig. 4 shows seven possible scenarios by which the incident radiation can release its energy within the three layers of the detector. Energy absorption can be from a single gamma-ray, a single beta particle or from both in coincidence. Corresponding to each interaction scenario shown in Fig. 4, seven possible pulse shapes or types could be generated at the PMT's anode output.

When the phoswich detector is exposed to a mixed beta-gamma source such as xenon radioisotopes, one can use anode pulses generated from scenario 3 (Fig. 4) to reconstruct beta-gamma coincidence spectra [23-25]. Therefore, we must first identify and discriminate this event from others. Then by calculating the areas under corresponding scintillation components (e.g. BC-400 and CsI(Tl)), a beta-gamma coincidence spectrum can be collected.

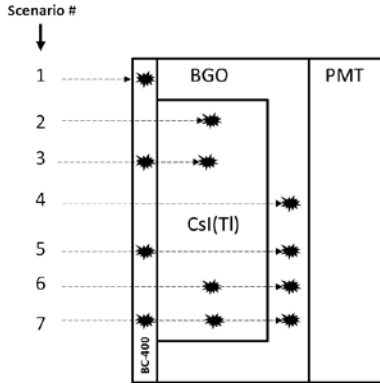


Fig. 4. Seven possible interaction scenarios either by incident beta or gamma-rays within scintillation layers of the phoswich detector.

To discriminate between different pulse shapes, the area under each anode pulse is calculated over three different time intervals (shown in Fig. 5) using three digital triangular filters with appropriate peaking times. y_1 , y_2 and y_3 traces shown in Fig. 5 are the responses of these filters to a typical phoswich signal pulse.

The output of the triangular filter, $y[n]$, used in this work (with negative-going input pulses) can be explained by the following general trapezoidal equation:

$$y[n] = \sum_{i=0}^{L-1} \{x[n-i-M] - x[n-i]\} \quad \text{Eq.1}$$

In the above equation, $x[n]$ is the input signal, $L.T$ is the peaking time where T is the sampling period, n is the sample number, and $M=L$ if the filter is a triangular filter with no flat top [26]. The output of this filter has a symmetric triangular shape when a step signal is applied to its input. The amplitude of $y[n]$ is equal to the area under the input pulse within the duration of the peaking time. The filter can be implemented using either FIR filters or recursive hardware-based digital processing. Since we used an offline analysis in this work, we employed FIR filters to implement this process.

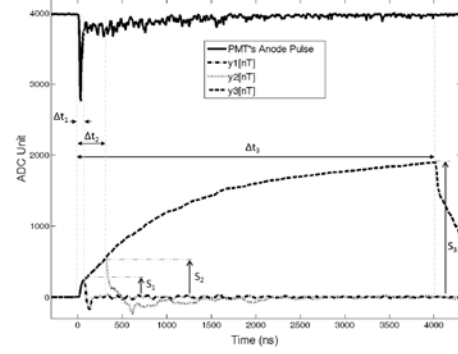


Fig. 5. A typical phoswich pulse when a coincidence event occurs in the detector. For each captured pulse, during three time intervals (Δt_1 , Δt_2 and Δt_3), three sums (S_1 , S_2 , and S_3) are calculated to discriminate between different events and measure the energy released in each phoswich layer. The pulse shown in this Fig. was captured with a sampling period (T) of 5 ns.

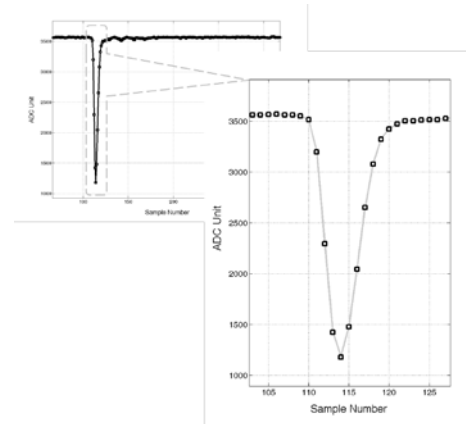


Fig. 6. A typical fast pulse from the BC-400 plastic scintillator captured with RX1200. The pulse was captured with a sampling period (T) of 5 ns.

Our measurements with pure beta emitters show that fast pulses from the BC-400 return to the baseline level after about 60 ns from the leading edge trigger (Fig. 6). In fact, the total time-constant of the readout input circuitry and the PMT stretches them to a longer duration when compared to the BC-400's scintillation decay constant (2.4 ns). Therefore, the peaking time of the first filter was set to be 60 ns to calculate the whole area under fast pulses from the BC-400. To cover the timing components from the BGO and CsI(Tl), the peaking times of the two other filters were chosen to be 300 ns and 4000 ns, respectively. The output amplitude of the three filters, S_1 , S_2 and S_3 shown in Fig. 5, represent the area or sum of each pulse 60 ns, 300 ns and 4000 ns after the trigger point, respectively. In Fig. 5, these three time intervals are indicated as Δt_1 , Δt_2 and Δt_3 .

Using these sums, two ratios, the Fast Component Ratio (FCR) and Slow Component Ratio (SCR) are calculated from each captured pulse. The FCR and SCR are calculated using the following Equations:

$$FCR = S_1 / S_2 \quad \text{Eq. 2}$$

$$SCR = (S_2 - S_1) / (S_3 - S_1) \quad \text{Eq. 3}$$

Since sum S_1 is a fraction of sum S_2 and both sums S_1 and S_2 are fractions of sum S_3 , the FCR and SCR defined in Equations 2 and 3 can range from zero to unity. Both $FCR=S_1/S_2$ and $FCR=S_1/S_3$ can be used in our pulse-shape discrimination, though we used the former. For the SCR , however, we needed to build a ratio independent of S_1 (the fast component) to only monitor the tailing portion of each pulse. For this reason the S_1 is subtracted from both S_2 and S_3 in calculating the SCR . In this way, for different energy absorption in the BC400, the SCR 's position of an event in the FCR - SCR plot does not change.

Fig. 7 shows a two-dimensional scatter plot of the FCR and SCR when the phoswich detector was exposed to a ^{137}Cs source. In this experiment, to locate coincidence events only due to Compton scattering between the three layers, the ^{137}Cs source was shielded against beta and conversion electrons. Depending on how the incident gamma-ray releases its energy within each layer of the phoswich detector, seven possible regions will be populated in the FCR - SCR scatter plot. Each region number, shown in Fig. 7, corresponds to the same scenario number illustrated in Fig. 4. Regions 1, 2 and 4 represent single events in plastic (BC-400), CsI(Tl) and BGO, respectively. Regions 3 and 5 are populated by CsI(Tl)-plastic and BGO-plastic coincidence events, respectively. Region 6 accommodates Compton scattering events between CsI(Tl) and BGO. When either all three timing components appear in the pulse or the shape of pulse is unknown, the corresponding event appears in region 7.

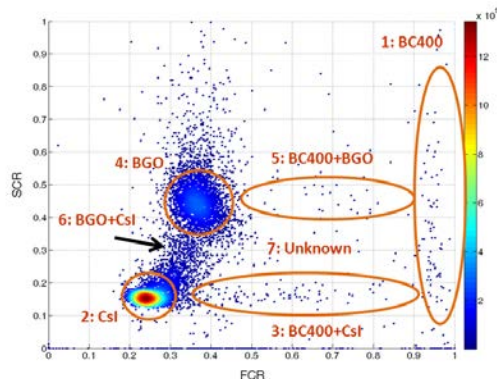


Fig. 7. Scatter of the Fast and Slow Component Ratios from ^{137}Cs . Seven marked regions correspond to seven pulse shapes, indicating how gamma-rays interact with the three layers of phoswich detector.

Since region 3, indicated in Fig. 7, is populated by the coincidence events occurring in the BC-400 and the CsI(Tl) but not in the BGO, events in this region are processed to construct our beta/gamma coincidence energy spectra. That is, we accept beta (BC400)/gamma (CsI(Tl)) coincidence events only if no energy absorption occurs in the BGO. A Compton scattering in the CsI(Tl) with a subsequent energy absorption in the BGO will remove the event from region 3. From the gamma-ray spectroscopy perspective, this is equivalent to an anti-coincidence logic commonly used in Compton suppression systems.

In this work, a user-programmable 12-bit/200 MHz digital pulse processor (RX1200, Avicenna Instruments LLC) was used to digitally process anode pulses from the phoswich detector. In all following measurements, the phoswich anode output was directly connected to the input of the digital pulse processor. In the RX1200, detector pulses are amplified and filtered in an analog conditioning circuit before being digitally sampled by a fast Analog-to-Digital Converter (ADC). In the analog conditioning stage, a third-order low-pass Bessel filter (anti-aliasing filter with a cutoff frequency of 90 MHz) is used to remove high-frequency components from the input signal.

For development purposes, in all measurements except for measuring the Suppression Factor, an offline digital analysis method was employed in MATLAB environment.

VI. MEASUREMENT RESULTS

A. Background count rate and energy resolution

To measure the background count rate, the phoswich detector was placed in a lead enclosure with a wall thickness of 5.0 cm. The total background count rate from all events was measured to be 3.29 counts per seconds. Our background measurements showed that the coincidence events in region 3 have a rate of 0.06 counts per second. The background count rates measured in other radioxenon detectors are provided in Table 3.

Table 3 also provides a comparison between the energy resolution (FWHM) of several gamma-rays measured in this work and in other major radioxenon detectors. Comparing with other standard radioxenon detectors, our measurements with the phoswich detector show poor resolutions for low energy gamma-rays (Table 3). The resolution of 662 keV of ^{137}Cs in the phoswich detector (8.9%), however, is better than that of the ARSA system (12%).

TABLE 3
ENERGY RESOLUTION (FWHM) AND BACKGROUND COUNT RATES FOR THE PHOSWICH AND MAJOR RADIOXENON DETECTORS.

	Detection System	Phoswich (this work)	SAUNA [2]	ARSA [27]	BGW [28]
Energy Resolution (%)	30 keV (^{137}Cs)	46.0	23-30	32	17
	88 keV (^{109}Cd)	25	14	NA	14
	122 keV (^{57}Co)	24	NA	22	13
	662 keV (^{137}Cs)	8.9	7.3	12	8.7
Background Rate (counts/s)	Total (all events)	3.29	7.5-12	30	5.5
	Coincidence Events	0.06	0.03	0.1	0.025

NA: data is not available

In this work, the gamma energy calibration for the CsI(Tl) was performed using ^{109}Cd (88 keV), ^{152}Eu (344 keV) and ^{137}Cs (662 keV) gamma-ray sources. The beta energy calibration for the BC400 was made using the endpoint energy of beta sources such as ^{99}Tc (292 keV) and ^{36}Cl (709 keV).

B. Study of Compton Suppression Mechanism

To study the Compton suppression mechanism of the phoswich detector, a suppression factor was defined as:

$$\text{SuppressionFactor}(E) = \frac{C_u(E) - C_s(E)}{C_u(E)} \quad \text{Eq. 4}$$

where $C_u(E)$ is the number of counts in energy E of the unsuppressed spectrum and $C_s(E)$ is the number of counts in energy E of the suppressed spectrum.

In this section, a simple lead collimator (Fig. 8) was used to expose the central area of the detector with 662 keV gamma-rays of ^{137}Cs (1.5 μCi) and collect the suppressed and unsuppressed gamma-ray spectra. ^{137}Cs is commonly used to characterize traditional Compton Suppression systems. The aperture in this collimator was 16 mm in diameter. The main role of this collimator was to target only the central portion of CsI(Tl) crystal and avoid direct interactions with the BGO.

We were able to obtain the best estimate of the suppression factor (as a function of energy) when we collect separate gamma-ray spectra with and without the BGO crystal. The first and second measurements give the suppressed and unsuppressed spectra, respectively. Another alternative for collecting the two spectra is to use the current phoswich configuration but use different regions for updating the suppressed and unsuppressed spectra.

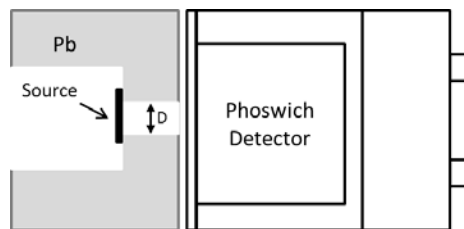


Fig. 8. Collimation arrangement used to collect suppressed and unsuppressed gamma-ray spectra from ^{137}Cs shown in Fig. 9.

Region 2 in Fig. 7 is populated from single events in CsI(Tl) (primarily from photoelectric interactions), thus events in this region can be used to collect a gamma spectrum with minimum Compton scattering in the CsI(Tl) crystal (suppressed spectrum).

To collect the unsuppressed gamma spectrum, events in both regions 2 and 6 can be used because in case of a Compton scattering in the CsI(Tl) and a consequent energy absorption in the BGO, the corresponding event moves from region 2 to region 6. Moreover, to collect the unsuppressed spectrum and to minimize the BGO contribution, only the area under tailing portion of each pulse should be calculated (see below).

The suppressed and unsuppressed gamma-ray spectra from ^{137}Cs (Fig. 10) were collected using an entirely real-time digital pulse processing algorithm implemented in an on-board Field-Programmable Gate Array (SPARTAN-3, XC3S1000). To collect these spectra, a 4096 x 32-bit energy histogram was realized from eight Block RAM memories in the FPGA. In each spectrum collection, the histogram was updated only if the measured $FCR-SCR$ values of the pulses fell into a predetermined $FCR-SCR$ region (region 2 for the suppressed and region 2+6 for the unsuppressed spectra).

As mentioned earlier, to minimize the BGO contribution in measuring the corresponding energy absorption in the CsI(Tl) crystal, only the area under the tailing portion of each pulse was calculated (500 nanoseconds to 5,000 nanoseconds after the trigger). This approximation degrades the CsI(Tl) energy resolution due to an incomplete pulse integration process. Moreover, a small contribution from the BGO crystal is observed in the low-energy region (below 170 keV) of the unsuppressed gamma spectrum (Fig. 9). However, both spectra in Fig. 9 show two peaks at low-energy region: a 30 keV x-ray peak from ^{137m}Ba and a 78 keV characteristic x-ray peak from the lead shield. A fraction of events in the second peak is suspected to be from fluoresced Bi X ray in the BGO. The energy resolution (FWHM) of the 662 keV peak in both spectra shown in Fig. 9 was measured to be 9.4%.

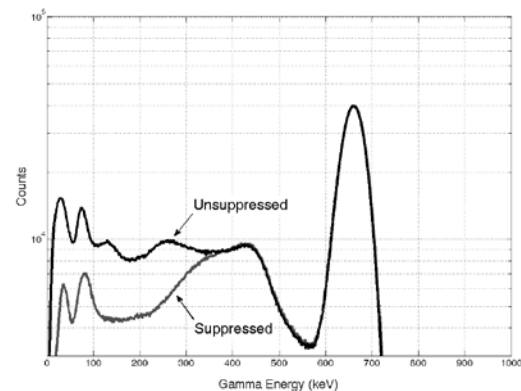


Fig. 9. Suppressed and unsuppressed gamma-ray spectra from ^{137}Cs .

Fig. 10 shows the resulting Suppression Factor plot as a function of photon energy using data presented in Fig. 9. In this Fig., fluctuations in the Suppression Factor (below about 170 keV) are mainly caused by the BGO contribution into the unsuppressed CsI(Tl) energy spectrum. Ignoring this portion of the plot, Fig. 10 shows that the Compton suppression

mechanism for the 662 keV gamma ray is more efficient (20%-50%) in the low-energy region of the Compton continuum (<300 keV) than that of close to the Compton edge (~477 keV). The characteristic shape of the Suppression Factor as a function of energy reflects the fact that because the CsI(Tl) crystal is not surrounded by the BGO crystal at the front window, the BGO is more efficient in detecting low-angle scattered photons from the CsI(Tl) scintillator. Events very close to the Compton edge correspond to scattering events at approximately 180-degrees and are more likely to escape the detector without releasing any detectable energy in the BGO.

For a given gamma energy, the amount of Compton suppression is a function of the BGO's thickness. Particularly for high-energy gamma-rays, the effect of the BGO's thickness is significant in the Compton suppression. However, for a given PMT size, increasing the thickness of the BGO will decrease the front area of the CsI(Tl) crystal and consequently will decrease the overall absolute efficiency.

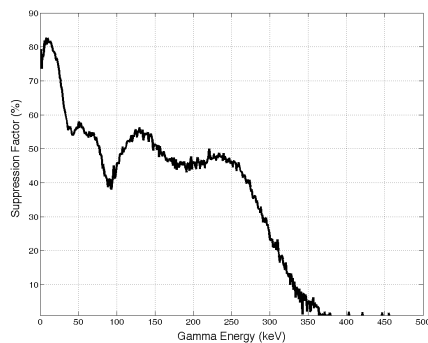


Fig. 10. Suppression Factor as a function of photon energy.

C. Radioxenon production

To test the detector for measuring xenon radioisotopes (^{135}Xe and ^{133}Xe), small volumes (3 ml) of stable and enriched (>99%) isotopes of xenon, ^{134}Xe and ^{132}Xe , were irradiated in the thermal column of the Oregon State University TRIGA reactor for two hours. The thermal neutron flux for this irradiation was $7 \times 10^{10} \text{ n.cm}^{-2}.\text{s}^{-1}$. The resulting activities for ^{135}Xe and ^{133}Xe at the time of gas injection into the detector were calculated to be 3.1 kBq and 14.8 kBq, respectively.

Designing a simple but efficient method to transfer a small amount of xenon gas to the reactor and from there to the phoswich detector was essential for our radioxenon production and detector characterization work [24]. The simplest method was to transfer the stable xenon gas from its storage vessel into a 3 ml disposable polypropylene syringe. The syringe, containing xenon gas, was then activated in the thermal column of the OSU's TRIGA reactor. After a cooling time, the activated xenon gas was then injected into the phoswich detector. Polypropylene syringes mainly contain hydrocarbons

and do not produce a significant amount of activity from neutron irradiation.

D. ^{135}Xe measurements

Fig. 11 presents the *FCR-SCR* scatter plot when the phoswich detector was exposed to ^{135}Xe (9.14 hours half-life). All major pulse-shape regions including the beta-gamma coincidence region (region 3, when both the BC-400 and CsI(Tl) crystal detect coincident energy absorption) can be identified in this Fig. The scatter plot shows that region 4 (BGO single events) is much more heavily populated than region 2 (CsI(Tl) single events). This did not agree with our previous radiation transport modeling. By examining the detector following the measurements, we noticed that the radioxenon gas had leaked from the gas cell into the space between scintillation assembly and aluminum housing during the measurement. This exposed the external surface of the BGO crystal directly to both beta and gamma radiation and resulted in a direct energy absorption in this layer. This problem was fixed for the rest of these experiments by filling the gap using a general purpose insulating foam sealant.

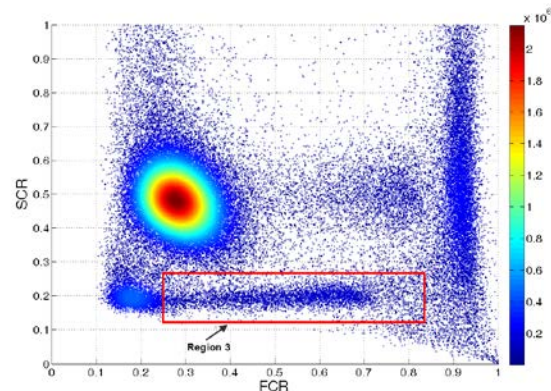


Fig. 11. Scatter of Fast and Slow Component Ratios from ^{135}Xe .

The resulting 3-D beta-gamma coincidence energy spectrum from ^{135}Xe is shown in Fig. 12. The horizontal plane in this Figure represents energy deposition in BC-400 and CsI(Tl). ^{135}Xe emits 250 keV gamma-rays in coincidence with beta particles ($E_{\beta\text{max}}=905 \text{ keV}$). Fig. 12 shows a populated area at a fixed gamma energy (250 keV photopeak) extending from zero to the maximum energy of beta particles.

The gamma-ray energy spectra from region 2 (suppressed, single events) and region 3 (suppressed, coincidence events) are shown in Fig. 13. The dashed spectrum in Fig 13 is a projected view of the gamma spectrum shown in Fig. 12. The single-event suppressed gamma-ray spectrum from our previous MCNP modeling work [14] is shown in Fig. 13 as a reference.

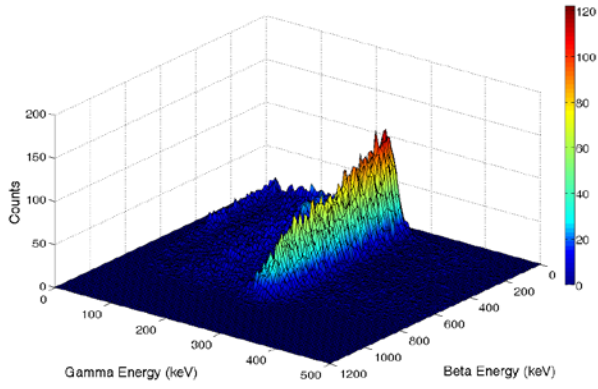


Fig. 12. 3-D beta-gamma coincidence energy histograms from ^{135}Xe .

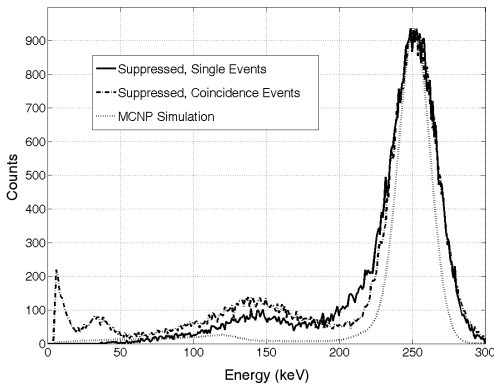


Fig. 13. The gamma energy spectra of ^{135}Xe in CsI(Tl). The solid and dashed spectra were updated from events in regions 2 (single events) and 3 (coincidence events), respectively. The gray spectrum is a suppressed single-event spectrum in CsI(Tl) and was obtained from our MCNP modeling [25].

Whereas the 250 keV photopeak in the simulated spectrum shown in Fig. 13 has a resolution (FWHM) of about 10%, the resolution for the same peak in both experimental spectra was measured to be 13%. A small peak at about 40 keV in the suppressed-coincidence spectrum is believed to be due to mischaracterization of low-energy BGO events into region 3. In our previous MCNP modeling work [25], no threshold was set for anti-coincidence logic (suppression process). This might be a reason why the shape of the experimental and simulated spectrum is different around the Compton edge. When high-angle and low-energy scattered photons from CsI(Tl) are absorbed in the BGO, it produces very small flashes (BGO has a low light yield comparing with CsI(Tl)) and may not be correctly detected and discriminated by the pulse shape discrimination process. This problem can be minimized by improving the overall light collection efficiency.

E. ^{133}Xe measurements

Fig. 14 shows the FCR-SCR scatter plot after ^{133}Xe (5.24 days half-life) was injected into the gas cell of the phoswich detector. The ^{133}Xe scatter plot shows many more events in

region 1 (BC-400 signal events) and in region 3 (CsI-BC400 coincidence events) than in other regions. Here, region 4 (BGO single events) is clearly identified and isolated from other regions but has a wider distribution when it is compared with the ^{135}Xe scatter plot. This may be related to its lower gamma energy (30 keV and 81 keV) which ultimately results in more uncertainty in the pulse shape discrimination process.

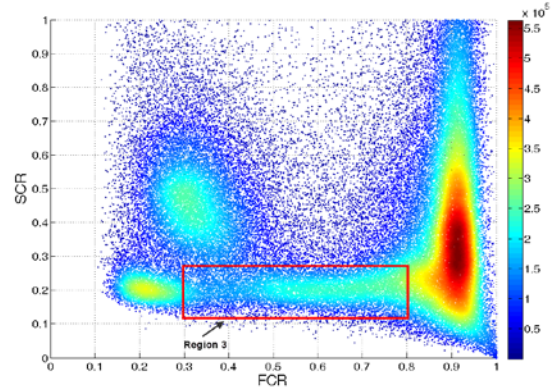


Fig. 14. Scatter of Fast and Slow Component Ratios from ^{133}Xe .

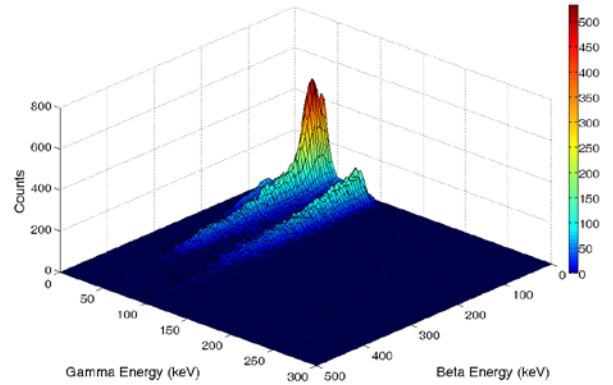


Fig. 15. 3-D beta-gamma coincidence energy histograms from ^{133}Xe .

The 3-D beta-gamma coincidence energy spectrum from ^{133}Xe is shown in Fig. 15. The horizontal plane in Fig. 15 represents energy absorption in BC-400 and CsI(Tl). In this Fig., 30 keV X-ray and 81 keV gamma-ray are clearly populated and extended up to the maximum energy of beta particles from ^{133}Xe .

Fig. 16 shows the beta-gated gamma-ray spectrum (projected view of the gamma spectrum shown in Fig. 15) from ^{133}Xe . This spectrum was collected using events in region 3 (beta-gamma coincidence events) of the FCR-SCR scatter plot. The energy resolution (FWHM) for 30 keV and 81 keV peaks were measured to be 46% and 24%, respectively. In this spectrum, events below about 15 keV are from electrical noise.

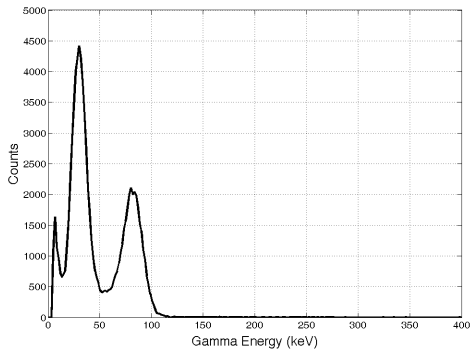


Fig. 16. Gamma energy spectrum in CsI(Tl) from ^{133}Xe . The spectrum was collected from events in region 3 (beta-gamma coincidence).

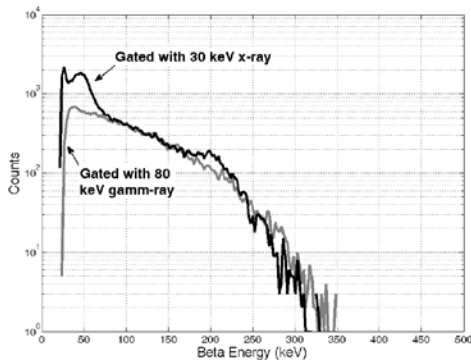


Fig. 17. Beta energy histograms (BC-400) from ^{133}Xe in plastic scintillator gated with 30-keV X-rays and 81-keV gamma-rays.

The beta energy spectra gated with two regions of interest in the gamma energy spectrum of ^{133}Xe , 30 keV and 81 keV, are shown in Fig. 17. The solid black spectrum was processed from events in region 3 (beta-gamma coincidence events) when a beta event from the BC-400 is detected in coincidence with a 30 keV x-ray from the CsI(Tl). The 30 keV-gated beta spectrum shows a peak at about 45 keV. This peak represents conversion electrons emitted in coincidence with 30 keV x-rays from ^{133}Xe . This sample was measured about 48 hours after the neutron irradiation. The presence of $^{133\text{m}}\text{Xe}$ (2.19 days half-life) can be confirmed by observing a small peak (from conversion electrons) at about 199 keV. The solid gray energy spectrum in Fig. 17 was processed from events in region 3 (beta-gamma coincidence events) when a beta event from the BC-400 is in coincidence with an 81 keV gamma-ray from the CsI(Tl). The 81 keV-gated beta energy spectrum shows a beta continuum with no peak, as expected.

VII. CONCLUSION

A phoswich detector with Compton suppression capability for radioxenon measurements via beta-gamma coincidence technique was developed and characterized. A fully digital pulse processing algorithm was developed to discriminate between different pulse shapes and to identify coincidence events in the detector. The results from our recent measurements with lab sources and radioxenon gases generated in the Oregon State University TRIGA reactor were

presented in this paper. Our recent measurements show that the Compton suppression mechanism reduces the Compton continuum from 662 keV photons by 20%-50% in the low-energy region of spectrum. Our beta-gamma coincidence measurements with ^{135}Xe and ^{133}Xe radioisotopes showed energy resolutions (FWHM) of 13%, 46% and 24% for 250 keV, 30keV and 80 keV gamma-ray peaks, respectively. More future works will be performed to enhance the overall performance of the phoswich detector, these will include (1) reassembling the phoswich detector with high-reflective wrapping materials and a high-gain PMT to improve overall signal-to-noise ratio, and (2) implementation of the current off-line digital pulse processing in the on-board FPGA device to achieve fast, real-time xenon measurements.

REFERENCES

- [1] E. Browne, R. B. Firestone, *Table of Radioactive Isotopes*, John Wiley and Sons, Inc., New York, 1986.
- [2] A. Ringbom, T. Larson, A. Axelson, K. Elmgren, and C. Johanson, "SAUNA - a system for automatic sampling, processing and analysis of radioactive xenon," *Nucl. Instr. and Meth. in Phys. Res. A*. vol. 508, p. 542, 2003.
- [3] J. P. Fontaine, F. Pointurier, X. Blanchard and T. Taffary, "Atmospheric xenon radioactive isotope monitoring," *J. of Environmental Radioactivity* vol. 72, p. 129, 2004.
- [4] P. L. Reeder and T. W. Bowyer, "Xe isotope detection and discrimination using beta spectroscopy with coincident gamma spectroscopy," *Nucl. Instr. and Meth. in Phys. Res. A*. vol. 408, p. 582, 1998.
- [5] T. W. Bowyer, K. H. Abel, C. W. Hubbard, A. D. McKinnon, M. E. Panisko, R. W. Perkins, P. L. Reeder, R. C. Thompson, R. A. Warner, "Automated separation and measurement of radioxenon for the Comprehensive Test Ban Treaty," *J. Radioanal. Nucl. Chem.* 235, p. 77, 1998.
- [6] J. Schulze, M. Auer, R. Werzi, "Low level radioactivity measurement in support of the CTBTO, *Applied Radiation and Isotopes*, vol. 53, p. 23, 2000.
- [7] J. I. McIntyre, T. W. Bowyer and P. L. Reeder, "Calculation of minimum detectable concentration levels of radioxenon isotopes using the pnnl ARSA system," Pacific Northwest National Laboratory, Technical Report PNNL-13102, 2006.
- [8] S. Usuda, H. Abe, A. Mihara, "Phoswich detectors combining doubly or triply ZnS(Ag), NE102A, BGO and/or NaI(Tl) scintillators for simultaneous counting of alpha, beta and gamma rays," *Nucl. Instr. and Meth. in Phys. Res. A*, vol. A340, p. 540, 1994.
- [9] S. Usuda, S. Sakurai, K. Yasuda, "Phoswich detectors for simultaneous counting of alpha -, beta (gamma)-rays and neutrons," *Nucl. Instr. and Meth. in Phys. Res. A*, vol. A388, p. 193, 1997.
- [10] T. L. White, W. H. Miller, "A triple-crystal phoswich detector with digital pulse shape discrimination for alpha/beta/gamma spectroscopy," *Nucl. Instr. and Meth. in Phys. Res. A*, vol. A422, p. 144, 1999.
- [11] N. L. Childress, W. H. Miller, "MCNP analysis and optimization of a triple crystal phoswich detector," *Nucl. Instr. and Meth. in Phys. Res. A*: vol. A490, p. 263, 2002.
- [12] B. H. Erkkila, M. H. Wolf, V. Eisen, W. P. Unruh, R. J. Brake, "A beta-gamma discriminator circuit," *IEEE Trans. Nucl. Sci.* vol. NS-32, no. 1, p. 969, 1985.
- [13] W. K. Warburton, M. Momayezi, B. Hubbard-Nelson, W. Skulski, "Digital pulse processing: new possibilities in nuclear spectroscopy," *Applied Radiations and Isotopes*, vol. 53(4-5), p. 913, 2000.
- [14] R. T. Schiffer, R. T., M. Flaska, S. A. Pozzi, S. Carney and D. D. Wentzloff, "A scalable FPGA-based digitizing platform for radiation data acquisition," *Nucl. Instr. and Meth. in Phys. Res. A*, Vol. 652, p. 491, 2011.
- [15] M. Nakhostin, "Recursive algorithms for digital implementation of neutron/gamma discrimination in liquid scintillation detectors," *Nucl. Instr. and Meth. in Phys. Res. A*, vol. 672, pp. 1, 2012.

- [16] H. Tan, M. Momayezi, A. Fallu-Labruyere, Y. X. Chu, and W. K. Warburton, "A fast digital filter algorithm for gamma-ray spectroscopy with double-exponential decaying scintillators," *IEEE Trans. Nucl. Sci.* vol. 51, no. 4, pp. 1541, 2004.
- [17] J. H. Ely, C. E. Aalseth, J. C. Hayes, T. R. Heimbigner, J. I. McIntyre, H. S. Miley, M. E. Panisko, and M. Ripplinger, "Novel Beta-gamma coincidence measurements using phoswich detectors," in *Proceedings of the 25th Seismic Research Review – Nuclear Explosion Monitoring: LA-UR-03-6029*, p. 533, 2003.
- [18] W. Hennig, H. Tan, W. K. Warburton, and J. I. McIntyre "Digital pulse shape analysis with phoswich detectors to simplify coincidence measurements of radioactive xenon," in *Proceedings of the 27th Seismic Research Review: Ground-Based Nuclear Explosion Monitoring Technologies*, LA-UR-05-6407, p. 787, 2005.
- [19] A.M. Baxter¹, T.L. Khoo, M.E. Bleich², M.P. Carpenter, I. Ahmad, R.V.F. Janssens, E.F. Moore³, I.G. Bearden, J.R. Beene, I.Y. Lee, "Compton-suppression tests on Ge and BGO prototype detectors for GAMMASPHERE," *Nucl. Instr. and Meth. in Phys. Res. A.* vol. 317, p. 101, 1992.
- [20] J. I. McIntyre, K. H. Able, T. W. Bowyer, J. C. Hayes, T. R. Heimbigner, M. E. Panisko, P. L. Reeder, and R. C. Thompson, "Measurements of ambient radioxenon levels using the automated radioxenon sampler/analyzer (ARSA)," *J. Radioanal. Nucl. Chem.* 248, p. 629, 2001.
- [21] C. E. Seifert, J. I. McIntyre, K. C. Antolick, A. J. Carman, M.W. Cooper, J. C. Hayes, T. R. Heimbigner, C. W. Hubbard, K. E. Litke, M. D. Ripplinger, and R. Suarez, "Mitigation of memory effects in beta scintillation cells for radioactive gas detection," in *Proceedings of the 27th Seismic Research Review: Ground-Based Nuclear Explosion Monitoring Technologies*, LA-UR-05-6407, p. 804, 2005.
- [22] G.F. Knoll, *Radiation Detection and Measurements*, Wiley, New York, 2000.
- [23] A. T. Farsoni and D. M. Hamby, "MCNP analysis of a multilayer phoswich detector for beta particle dosimetry and spectroscopy," *Nucl. Instr. and Meth. in Phys. Res. A.* vol. 555(1-2), p. 225, 2005.
- [24] A. T. Farsoni and D. M. Hamby, "Characterizing a two-channel phoswich detector using radioxenon isotopes produced in the OSU TRIGA reactor," in *Proceedings of the 2010 Monitoring Research Review: Ground-Based Nuclear Explosion Monitoring Technologies*, LA-UR-10-05578, p. 585, 2010.
- [25] A. T. Farsoni and D. M. Hamby, "Design and modeling of a Compton-suppressed phoswich detector for radioxenon monitoring," in *Proceedings of the 2010 Monitoring Research Review: Ground-Based Nuclear Explosion Monitoring Technologies*, LA-UR-10-05578, p. 595, 2010.
- [26] V. T. Jordanov and G. F. Knoll, "Digital Synthesis of pulse shapes in real time for high resolution radiation spectroscopy," *Nucl. Instr. and Meth. in Phys. Res. A*, vol. A345, p.337, 1994.
- [27] P. L Reeder, T. W. Bowyer, J. I. McIntyre, W. K. Pitts, A. Ringbom, and C. Johansson, "Gain calibration of coincidence spectrometer for automated radioxenon analysis," *Nucl. Instr. and Meth. in Phys. Res. A*, vol. A521, p.586, 2004.
- [28] M. W. Cooper, , J. I. McIntyre, T. W. Bowyer, A. J. Carman, J. C. Hayes, T. R. Heimbigner, C. W. Hubbard, L. Lidey, K. E. Litke, S. J. Morris, M. D. Ripplinger, R. Suarez, R. Thompson, "Redesigned β - γ radioxenon detector," *Nucl. Instr. and Meth. in Phys. Res. A*, vol. A579, p.426, 2007.